Assessing Degradation-Aware Model Predictive Control for Energy Management of a Grid-Connected PV-Battery Microgrid

Alan Gen Li
Department of Electrical Engineering
Columbia University
New York, NY, USA
agl2142@columbia.edu

Matthias Preindl
Department of Electrical Engineering
Columbia University
New York, NY, USA
matthias.preindl@columbia.edu

***Abstract*—Grid-connected residential solar-photovoltaic (PV) and battery systems are increasingly popular types of microgrids. Determining the optimal energy management system (EMS) strategy for such microgrids depends on many factors, such as power demand, solar irradiation, and system costing. The energy flow for a residential PV-battery microgrid is thus studied in detail. Three algorithms are used, including load-levelling, peak-shifting, and an original model predictive control (MPC) EMS. PV cells, battery overpotentials and degradation are simulated with physically-meaningful models. Real data from Long Island, New York, are used to simulate the load power demand, solar irradiation, utility costs, degradation costs, and PV credits. Both load and PV forecasting error are considered. Results for the base cases demonstrate the advantage of MPC EMS. Simulation parameters are then varied to show that the simulated cost savings depend on the costing assumptions and forecasting error.**

***Index Terms*—Microgrids, Energy management, Photovoltaics, Battery storage, Battery degradation**

I. Introduction

Renewable energy integration is key to achieving greenhouse gas reduction goals [1]. Solar photovoltaics (PV) and lithium-ion batteries (LIB) are dominant technologies with falling costs and more installations [2], [3]. Renewable sources like PV, however, suffer from decentralized generation and intermittency. Microgrids, part of the smart grid framework, may offer a solution [4], [5]. Grid-connected PV-battery microgrids, represented in Fig. 1, are common arrangements [6]. Optimal operation of microgrids benefits users by increasing power reliability and reducing costs. They can also increase energy efficiency by avoiding alternating to direct current (AC to DC) conversion from the mains [7]. The main grid also benefits from better management of intermittent renewable energy sources and improved resilience.

Microgrids energy management systems (EMS) must determine the energy flow that will minimize the overall cost to the user or society [5], [8], [9]. The EMS controls battery charge scheduling, PV power export, and grid power imports. While the costs of using the grid and selling PV power are determined by the utility and the electricity spot market [10], the LIB cost depends on battery degradation. Battery degradation remains the subject of much research, but models of varying complexity are used to quantify lifetime accurately [11].

EMS may be centralized or decentralized [9]. Decentralized architectures are considered 'autonomous' because the microgrid components receive little to no instruction from a central controller. The units follow a certain strategy or act as decision-making agents [4]. While more resilient and often offering faster computation times, decentralized EMS strategies rely on high-performance interconnected communication networks. This increases system complexity and cost. Thus centralized architectures are still widely used.

Many EMS strategies have been developed [5]. Simple rule-based methods include load-levelling (LL) or self-consumption maximization, where the battery is used to store as much PV power as possible [3]. More advanced model-based methods use load and weather forecasting to perform peak shifting (PKS) or time-of-use arbitrage, which draws grid power during cheaper periods to avoid power use during the peak.

Model predictive control (MPC) is a popular centralized model-based EMS that can manage multiple constraints over dynamic time periods [7], [12], [13]. A MPC-based EMS determines the optimal control signals for a given future time horizon at each instance of optimization. Horizons can last from a few minutes to several hours or days. At the component level, MPC ensures that the load power demand and safe operation constraints are always met [13]. At the grid level, MPC minimizes the total operating cost based on predicted energy flows over the horizon. Optimization variables may include the battery charging rate and duration, grid use, or PV market participation. Since MPC may have long computation times, neural networks were used to replace the traditional discrete-recursive model definitions [7]. MPC has been used in numerous studies but it remains unclear whether it is always more cost-effective than a simpler EMS, or only in specific conditions.

To better understand the effects of different EMS strategies on system performance, we study three EMS algorithms applied to a residential PV-battery microgrid in Long Island

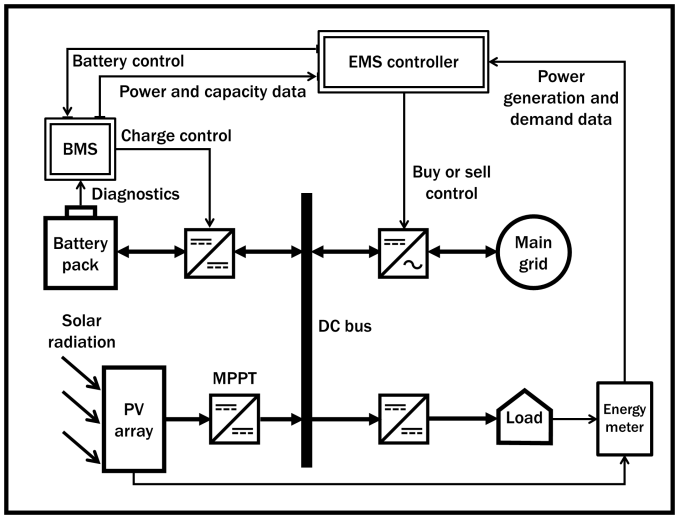

Fig. 1. Microgrid system diagram showing energy flow and components including the battery management system (BMS)

suburbs of New York. Real data is used to simulate system performance using LL, PKS, and MPC EMS, representing increasing levels of sophistication. Costs from the grid, battery degradation, and PV credit are derived and assessed using different assumptions. The novel RHD overpotential ECM is used to simulate the LIB cells [14]. We show that the benefits of the MPC EMS relative to LL or PKS depends on costing and modelling assumptions.

We continue in Section II to describe PV, battery, and EMS modelling. In Section III we describe our data and costing. In Section IV results are presented and discussed. We conclude in Section V.

II. System Design

A. Photovoltaic array modelling

PV power generation is proportional to the solar irradiation P_{sun} [Wm^{-2}] received by the panel. The array is modelled from the cell level using

$$I = I_p - I_s\left(e^{\frac{V}{nV_T}} - 1\right) - \frac{V}{R_{sh}} \tag{1}$$

where I is the cell current, V is the cell voltage, I_p is photocurrent (determined by P_{sun}), I_s is diode saturation current, V_T is the diode thermal voltage, R_{sh} is shunt resistance, and n is the diode ideality factor. Series resistance is assumed negligible.

We simulate a four-panel array with area 4 m^2, $N_s = 60$ cells per string, and $N_p = 8$ parallel branches (2 branches per panel). Assuming the cells are identical and operate in identical conditions, the array current and voltage are given by $I_{array} = N_p I$ and $V_{array} = N_s V$. A DC-DC converter is often used to control the cell voltage to obtain the maximum-power-point (MPP). We assume that the converter is lossless and that the PV system achieves MPP within one sampling interval.

B. Battery modelling

The EMS uses the newly-proposed RHD model [14], [15], an overpotential ECM linking diffusivity with battery state of health. The terminal voltage is given by

$$v(t_k) = V_{OC}(z, t_k) - V_s(t_k) - V_{ct}(t_k) - V_D(t_k) \tag{2}$$

where V_{OC} is the open-circuit voltage (OCV), $z(t_k)$ is the cell state of charge (SoC), t_k is the time at step k, and V_s, V_{ct}, and V_D are the solution, charge transfer, and diffusion overpotentials. Standard NRC equations govern V_s and V_{ct},

$$\begin{aligned} x_\ell(t_{k+1}) &= \left(e^{-\frac{\Delta t}{R_1 C_1}}\right) x_\ell(t_k) + \left(1 - e^{-\frac{\Delta t}{R_1 C_1}}\right) i(t_k) \\ V_{ct}(t_k) &= R_1 x_\ell(t_k), \qquad V_s(t_k) = R_0 i(t_k) \end{aligned} \tag{3}$$

with resistances R_0 and R_1, capacitance C_1, and sampling interval Δt. Note that each variable is a real integer when only 1 RC-pair is used. The diffusion overpotential is defined with $M = 2$,

$$\begin{aligned} x_\nu(t_{k+1}) &= A_\nu x_\nu(t_k) + B_v u(t_k) \\ V_D(t_k) &= C_\nu x_\nu(t_k) \end{aligned} \tag{4}$$

$$\begin{aligned} A_\nu &= \begin{pmatrix} 1 & \sqrt{1.5} & 0 & 0 \\ 0 & 0 & \sqrt{1.5} & 0 \\ 0 & 0 & 0 & \sqrt{2} \\ 0 & 0 & 0 & 0 \end{pmatrix} \\ B_\nu &= \frac{dV_{OC}(t_k)}{dz}\sqrt{\Delta t} \begin{pmatrix} 0 & 0 \\ 0 & 0 \\ 0 & 0 \\ 1 & -1 \end{pmatrix} \\ C_\nu &= A_D \begin{pmatrix} 1 & 1 & 1 & 1 \end{pmatrix} \end{aligned} \tag{5}$$

where $x_\nu \in \mathbf{R}^{M+2}$ is a column vector, $A_\nu(k)$ is a sparse square matrix with elements on the superdiagonal, B_ν is a tall sparse matrix with $M + 2$ rows and 2 columns, C_ν is a row vector, and A_D is the diffusion constant.

Given a power demand $P(t)$, the current and voltage must meet the demand at each time step,

$$P(t_k) = i(t_k) v(t_k) \tag{6}$$

Since the current input lags the state update vectors by 1 step, we substitute equations (2)-(5) into (6) then rearrange to obtain current from the quadratic equation,

$$i(t_k) = \frac{-V_{st} + \sqrt{V_{st}^2 - 4R_0 P(t_k)}}{-2R_0} \tag{7}$$

where we define V_{st} for concision,

$$V_{st} = V_{OC}(t_k) - V_{ct}(t_k) - V_D(t_k) \tag{8}$$

During discharge, $V_{st}^2 > 4R_0 P(t_k)$ for the equation to yield a real value. This reflects the maximum power transfer limit. During charge, $P < 0$ so the argument of the square root is always positive.

Battery degradation is modelled using simplified solid-electrolyte interface (SEI) layer dynamics at the negative electrode (NE) [16], assumed to be the dominant degradation

TABLE I
DEGRADATION MODEL PARAMETERS

Symbol	Definition	Value [units]
$J_{0,s}(z)$	Exchange current density, side	[Am^{-2}]
$U_n(\theta)$	NE equilibrium potential	[V]
$\theta(z)$	NE lithiation state	—
$J_0(z)$	Exchange current density, main	[Am^{-2}]
F	Faraday's constant	96485 [Cmol^{-1}]
U_s	Side reaction equilibrium potential	0.2 [V]
R	Ideal gas constant	8.314 [$\mathrm{Jmol}^{-1}\mathrm{K}^{-1}$]
T	Temperature	298 [K]
θ_{min}	Minimum lithiation	0.05
θ_{max}	Maximum lithiation	0.85
a_n	Volumetric density coefficient	1 [m^{-1}]
A_{neg}	NE cross-sectional area	0.0596 [m^2]
ℓ_{neg}	NE length	88 [μm]

mechanism [17]. This growth is quantified with a 'side-reaction' flux $j_s(t_k)$ that does not contribute to intercalation,

$$j_s(t_k) = \frac{AB + A\sqrt{B^2 + (1-2CA)}}{1-2CA} \tag{9}$$

$$\begin{aligned} A &= \frac{-J_{0,s}(z)}{F}\exp\left(\frac{F\big(U_s - U_n(\theta)\big)}{2RT}\right) \\ \theta &= \theta_{min} + z(t_k)\big(\theta_{max} - \theta_{min}\big) \\ B &= \frac{-i_{cell}(t_k)}{2a_n J_0(z) A_{neg}\ell_{neg}}, \qquad C = \frac{F}{2J_0(z)} \end{aligned} \tag{10}$$

where definitions of variables and constants are shown in Table I. A four-harmonic Fourier series interpolation of the data in [18] is used for J_0, assumed to be 4 orders of magnitude greater than $J_{0,s}$. NE equilibrium potential U_n is defined using the pseudo-OCV measurements from a graphite half-cell, with lithiation θ limited by θ_{min} and θ_{max}. Other constants are as listed in [19].

By assuming SEI formation dominance, side-reaction flux becomes directly proportional to the degradation rate. Total capacity $Q_T(t_k)$ is then calculated using

$$Q_T(t_k) = Q_T(t_{k-1}) + a_n A_{neg}\ell_{neg} F \Delta t j_s(t_k) \tag{11}$$

which shows degradation is exacerbated by high SoC and charging current. The equations governing the evolution of parameters with state of health (SoH) are given by

$$\begin{aligned} R_0 &= 0.25\Delta\mathrm{SoH} + 0.05, \quad R_1 = 0.45\Delta\mathrm{SoH} + 0.01 \\ C_1 &= 300\cdot 10^{2.301\Delta\mathrm{SoH}}, \quad A_D = \sqrt{e^{-(23-35\Delta\mathrm{SoH})}} \end{aligned} \tag{12}$$

where

$$\Delta\mathrm{SoH}(t_k) = 1 - \frac{Q_T(t_k)}{Q_T(0)} \tag{13}$$

In the battery pack, it is assumed that all cells are identical $N_s = 60$ cells per series module, and $N_p = 14$ branches in parallel so the pack voltage and current are given by $v_{pack} = N_s v$ and $i_{pack} = N_p i$. Nominal pack voltage $V_{pack}^{nom} = 50\,\mathrm{V}$ is equal to the value in [20]. Nominal cell voltage $V_{cell}^{nom} = 3.6\,\mathrm{V}$ is based on INR18650-20R characteristics [21]. Nominal pack capacity $Q_{pack}^{nom} = 10\,\mathrm{kWh}$ is comparable to average battery pack size in a residential household. Cell charging currents are limited to 3A, discharge currents are limited by the load demand, and SoC is limited to the range [0.05, 0.95].

C. Energy management strategies

The microgrid demands that the following equality constraint be met at each time-step:

$$P_L = P_{PV} + P_B + P_G \tag{14}$$

where P_L is the load demand, P_{PV} is the PV array output, P_B is the battery power output, and P_G is the power drawn from the grid. Grid power must be imported if the power supplied by the PV array and BESS do not meet the load demand. If $P_L < P_{PV}$, then PV power may be exported. The grid may also charge the battery if $P_B < 0$ and $|P_B| > P_{PV}$. All power electronics and transmission lines are assumed lossless, and microgrid control techniques are assumed to achieve perfect stability with instantaneous communication.

Since the LL EMS is rule-based, it operates the battery using

$$\begin{cases} \text{if } P_L - P_{PV} \geq 0, \quad P_B \geq 0 \\ \text{else } P_B \leq 0 \end{cases} \tag{15}$$

and draws grid power or allows PV power to be sold only when the battery is empty or full. It can be seen that LL encourages PV power to be stored in the battery but this may not minimize the total cost.

The model-based EMS use load and PV forecasting to inform the operating choices. Each day is divided into four periods, shown in Fig. 2, that can be used to characterize the EMS. Forecasting error for the load is represented using

$$\hat{P}_L(t_k) = a_w(t_k - t_0)P_L(t_k) + w(t_k) \tag{16}$$

where $\hat{(\cdot)}$ refers to predicted values, y is the true value, t_0 is the time at which the prediction is made, $a_w \in \mathbf{R}$ is a random normally distributed number generated at t_0, and $w(t) \in \mathbf{R}$ is additive white Gaussian noise. Thus the absolute load prediction error increases as the prediction horizon $(t_k - t_0)$ increases. Forecasting for PV generation is represented with

$$\hat{P}_{PV}(t_k) = |1 + a_w + 0.25w(t_k)|P_{PV}(t_k) \tag{17}$$

Since the sunrise and sunset times are well-known, PV forecasting error does not increase over time, but rather under- or over-predicts.

PKS uses energy forecasts to charge the battery in period 1 such that no grid power is needed during period 3 (peak). At the first sampling instance of the day, it estimates the load and PV energy difference during the day and during the peak, and the currently available energy in the battery pack,

$$\begin{aligned} \Delta E_{\mathrm{pk}} &= \int_{t_{\mathrm{rise}}}^{16\mathrm{h}} (\hat{P}_L - \hat{P}_{PV})dt - \int_{16\mathrm{h}}^{20\mathrm{h}} (\hat{P}_L - \hat{P}_{PV})dt \\ E_B &= zQ_T N_p V_{\mathrm{pack}}^{\mathrm{nom}} \end{aligned} \tag{18}$$

where t_{rise} is the sunrise time. If $\Delta E_{\mathrm{pk}} + E_B < 0$, then the EMS determines that there is insufficient energy to avoid grid power

Fig. 2. Four time periods used by the model-based EMS strategies, PKS and MPC

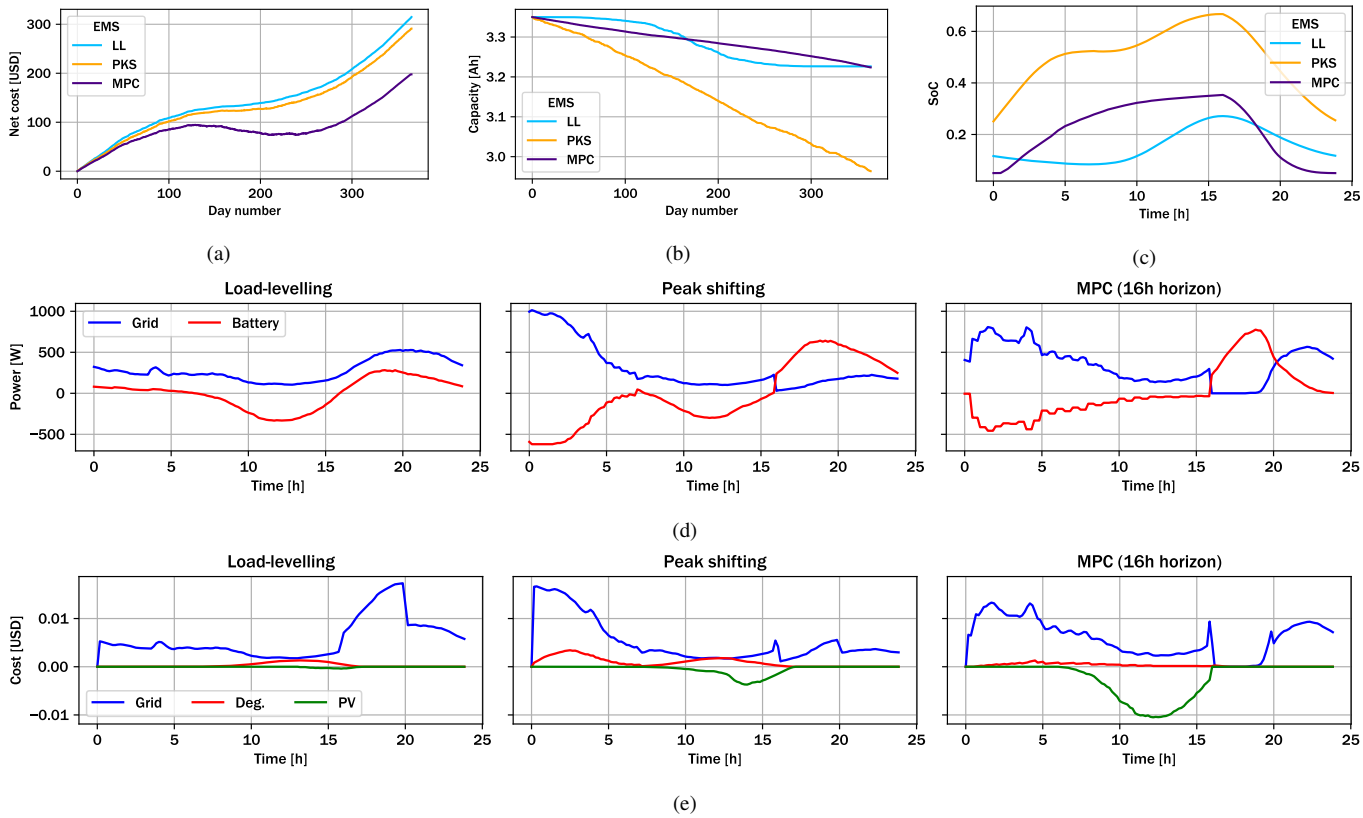

Fig. 3. Comparison between EMS algorithms for for base case costing and modelling assumptions, showing (a) Cumulative annual cost, (b) Battery capacity fade, (c) Average daily cell SoC, (d) Average daily power, and (e) Cost profiles

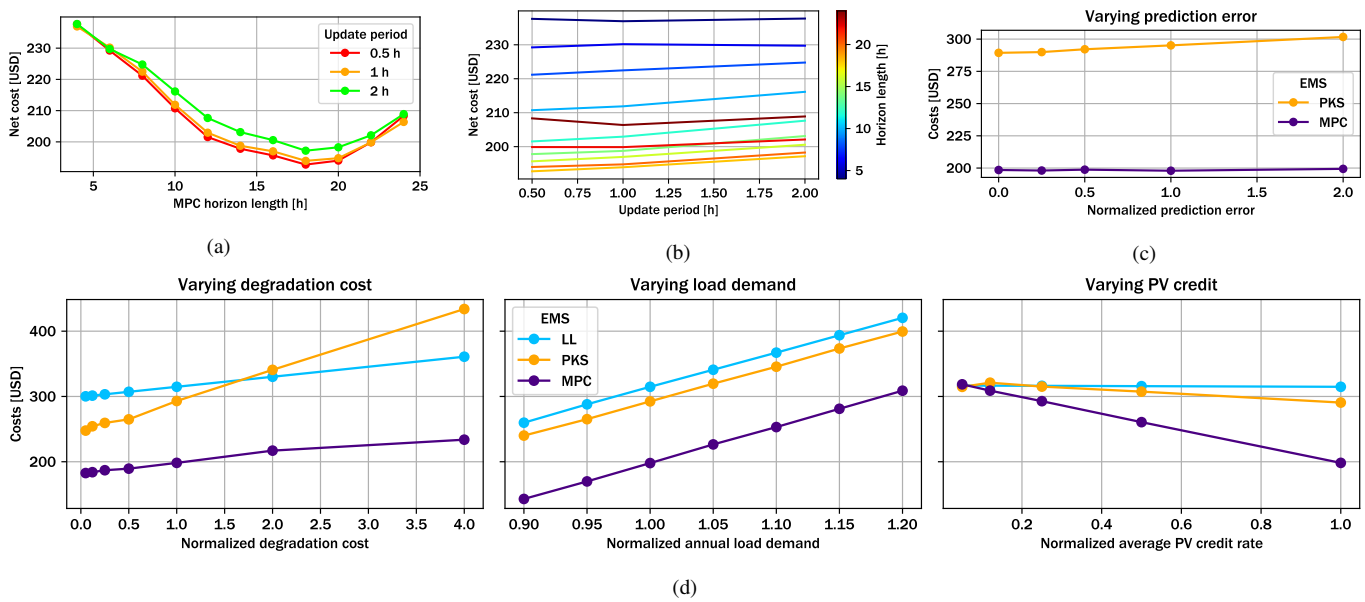

Fig. 4. Plots showing how net cost varies with simulation parameters relative to the reference base case assumptions, for (a) MPC horizon length, (b) MPC update period, (c) Prediction error, and (d) Degradation cost, Load demand, and PV credit,

during the peak. In this case the battery charged throughout period 1 at the rate

$$P_B(\text{period} = 1) = \frac{\Delta E_{\text{pk}} + E_B}{T_1} \tag{19}$$

where T_1 is the length of period 1 which varies according the time of sunrise. During period 4 it follows the LL rule. Thus PKS aims to minimize the amount of grid power drawn during the doubly expensive evening peak period.

The MPC EMS acts during periods 1 and 2 for a specific horizon length T_H and update period T_r. At each relative sampling instance r, it minimizes a cost function for all $k\Delta t = rT_r$ following

$$\begin{aligned} \text{minimize} \quad & f_{\text{cost}}(rT_r, T_H, P_B) \\ \text{subject to} \quad & P_L = P_{PV} + P_B + P_G \\ & -1000 \leq P_B \leq 0 \\ & \text{period} \in \{1, 2\} \end{aligned} \tag{20}$$

$$f_{\text{cost}} = c_{\text{grid}}\hat{P}_G^+ + c_{\text{deg}}\hat{\Delta Q}(T_H, P_B) + \hat{c}_{PV}|\hat{P}_G^-| \tag{21}$$

where $k, r \in \mathbf{Z}^+$, c_{grid}, c_{deg}, and c_{PV} are the rates for grid cost, degradation cost, and PV credit, $\hat{\Delta Q}$ is the predicted capacity loss over the horizon length, $(\cdot)^{\pm}$ refers to positive or negative values, c_{grid}, $\hat{c}_{PV}$ are row vectors and $\hat{P}_G$, $\hat{P}_L$ are column vectors of length $T_H/\Delta t$. Here, the optimal battery charging power $P_B^\star$ is obtained using a basic grid-search algorithm with tolerance 10 W. It can be seen that MPC is sensitive to several parameters, including cost weightings, horizon length, and update period. We thus examine several combinations of T_H and T_r, with reference values $T_H = 16\,\text{h}$ and $T_r = 30\,\text{min}$. Unlike the other EMS strategies, MPC explicitly considers the total system cost and aims to achieve the lowest value.

III. Data and Costing

We use real data to simulate the annual energy flow occurring in an average Long Island household in Nassau County, New York, in 2021. Annual household load data is obtained from [22] and scaled to match the average residential energy use in Long Island. We examine a variety of costing scenarios relative to the 'base cases'. One simulation parameter is changed while the others remain constant. Normalized values are defined using the reference load energy demand, PV credit, and degradation costs that are described below.

Grid costs are determined by the 4-hour peak option from the Long Island power authority [23], where grid power costs \$0.20 during the evening peak from 16:00 to 20:00, and an average of \$0.10 otherwise. Solar irradiation profiles for the Long Island area in 2021 were obtained from the National Solar Radiation Database [24].

The New York State Energy Research and Development Authority mandates that electric utilities provide credit to residents with PV installations based on the value of distributed energy resources (VDER) calculation [10]. The VDER is composed of the 'value stack', which quantifies the benefits from supplying PV power to the grid. The VDER is composed of market, capacity, environmental, and community credits [23]. The market rate [\$ MWh^{-1}] is determined by the day-ahead market locational-based marginal pricing reported by the New York Independent System Operator [25]. Other credits are combined to yield an additional credit of approximately \$136.03 MWh^{-1}.

Several methods have been used to quantify degradation cost, such as energy throughput [26] or number of cycles [3]. Assuming a replacement pack is ordered as soon as the battery pack loses 40% of original capacity, degradation cost can be derived purely from the capacity loss. There are, however, environmental, economic, and social benefits from battery storage that are beyond the scope of this report [27]. Thus a scaling factor is chosen to significantly reduce the cost to $c_{\text{deg}} = \$2.07\,\text{Ah}^{-1}$.

IV. Results and Discussion

Results using the reference parameters are shown in Fig. 3. It can be seen that the different EMS algorithms result in distinct profiles. From Fig. 3a we see that the highest cost is from LL. In Fig. 3b PKS degrades the battery most significantly. Annual costs can be explained by the average daily profiles in Figs. 3c-e.

In LL, the battery is charged using PV power around noon. Since there is no forecasting, the LL EMS suffers from high grid costs during the evening peak because the battery cannot meet the full load demand. In PKS, the battery is charged twice: first in the early hours and second around noon. This allows grid costs to be significantly reduced during the peak period and PV power to be exported. Some grid power is still drawn during the peak because of imperfect forecasting, which may also increase battery degradation due to the elevated SoC levels. In MPC, there is only one major charging period and the EMS minimizes battery use during the day, preferring to export PV power for credit. Thus MPC trades higher grid costs in the evening for significant PV revenue during the day.

In Fig. 4 the effects of costing and modelling assumptions can be clearly observed. First, in Figs. 4a-b, the net cost of MPC is strongly dependent on horizon length and lightly correlated with update period. MPC cost is minimized for horizon 18 h and half-hour update period. This shows the importance of parameter tuning for a given set of conditions. MPC is less sensitive to prediction error compared to PKS as shown in Fig. 4c, which may be explained by its consistent updates. In Fig. 4d, LL and MPC are equally sensitive to degradation cost, with PKS more severely affected. Changing the load demand affects all EMS equally. PV credit creates the most significant discrepancies. As the PV credit goes to 0, all the EMS have approximately equal costs This suggests that the advantage of using a model-based EMS disappears and may even be detrimental if there is no benefit to exporting PV power.

As expected, the lowest net cost is achieved by reducing degradation cost and load demand and increasing PV credit. Our results strongly indicate that model-based EMS are needed to fully exploit the cost benefits under these conditions. In other regions of the world besides our chosen example of Long

Island, New York, degradation costs may be higher and the PV credit may be reduced due to remoteness or geographical constraints. As our results show, a rule-based EMS like LL would be superior in these conditions.

Modelling assumptions create discrepancies with a real system. Power electronics losses and low-level converter control are important for components such as the PV array and would be important considerations. Errors in the degradation model may underestimate the effects of low SoC, positive electrode degradation, and temperature. Using a higher fidelity degradation model would likely increase costs in simulation but improve EMS performance in a real system [11].

V. Conclusion

A grid-connected PV-battery microgrid was simulated using real year-long data for an average household in Long Island, New York. Physics-derived models were used to simulate the PV array, battery overpotentials, and battery degradation. Costs are derived using market-based analysis. LL, PKS, and an original MPC EMS were formulated to understand the variation of net costs with a wide variety of simulation parameters. We show that model-based EMS strategies are not necessarily superior to simple rule-based EMS if degradation costs are too high or the PV credit rate is too low. Still, the MPC EMS most consistently results in the lowest costs.

There are several areas for future work. More comprehensive degradation modelling can be used. A lower sampling interval would allow effects of transient overpotentials to be examined. To verify simulated results, a laboratory-scale model could be created. In a real microgrid, savings could be obtained in a real household system with only a software update. In higher-cost regions, government subsidies can not only help reduce the market value of utility costs, battery degradation, or PV credits, but also allow advanced EMS algorithms to optimize the energy flow and reduce net costs even further.

References

[1] IPCC, "Climate change 2021: The physical science basis. contribution of working group I to the sixth assessment report of the intergovernmental panel on climate change," *Cambridge University Press*, 2021.

[2] A. G. Li, , A. C. West, and M. Preindl, "Towards unified machine learning characterization of lithium-ion battery degradation across multiple levels: A critical review," *Appl. Energy*, vol. 316, no. 119030, 2022.

[3] D. Azuatalam, K. Paridari, Y. Ma, M. Forstl, A. C. Chapman, and G. Verbic, "Energy management of small-scale pv-battery systems: A systematic review considering practical implementation, computational requirements, quality of input data and battery degradation," *Renew. Sus. Energy Reviews*, vol. 112, pp. 555–570, 2019.

[4] H. Kim, H. Choi, H. Kang, J. An, S. Yeom, and T. Hong, "A systematic review of the smart energy conservation system: From smart homes to sustainable smart cities," *Renew. Sus. Energy Reviews*, vol. 140, no. 110755, 2021.

[5] A. Hirsch, Y. Paraga, and J. Guerrero, "Microgrids: A review of technologies, key drivers, and outstanding issues," *Renew. Sus. Energy Reviews*, vol. 90, pp. 402–411, 2018.

[6] K. A. Plytaria, D. Steen, L. A. Tuan, O. Carlson, and M. A. F. Ghazvini, "Market-based energy management model of a building microgrid considering battery degradation," *IEEE Trans. Smart Grid*, vol. 12, no. 2, pp. 1794–1804, 2021.

[7] A. N. Akpolat, M. R. Habibi, H. R. Baghaee, E. Dursun, A. E. Kuzucuoglu, Y. Yang, T. Dragicevic, and F. Blaabjerg, "Dynamic stabilization of dc microgrids using ann-based model predictive control," *IEEE Trans. Energy Conversion*, 2022, in press.

[8] A. Muhtadi, D. Pandit, N. Nguyen, and J. Mitra, "Distributed energy resources based microgrid: Review of architecture, control, and reliability," *IEEE Trans. Industry Appl.*, vol. 57, no. 3, pp. 2223–2234, 2021.

[9] M. F. Zia, E. Elbouchikhi, and M. Benbouzid, "Microgrids energy management systems: A critical review on methods, solutions, and prospects," *Appl. Energy*, vol. 222, pp. 1033–1055, 2018.

[10] Joint Utilities New York. (2021) Value of Distributed Energy Resources (VDER). [Online]. Available: https://jointutilitiesofny.org/distributed-generation/VDER

[11] J. M. Reniers, G. Mulder, and D. A. Howey, "Unlocking extra value from grid batteries using advanced models," *J. Power Sources*, vol. 487, no. 229355, 2021.

[12] J. Hu, Y. Shan, J. M. Guerrero, A. Ioinovici, K. W. Chan, and J. Rodgriguez, "Model predictive control of microgrids – an overview," *Renew. Sus. Energy Reviews*, vol. 136, no. 110422, 2021.

[13] D. Y. Yamashita, I. Vechiu, and J. P. Gaubert, "Two-level hierarchical model predictive control with an optimised cost function for energy management in building microgrids," *Appl. Energy*, vol. 285, no. 116420, 2021.

[14] A. G. Li and M. Preindl, "Linear state-space modelling of the diffusion overpotential in li-ion batteries using a receding horizon," *Appl. Energy*, unpublished.

[15] A. G. Li, K. Mayilvahanan, A. C. West, and M. Preindl, "Discrete-time modeling of li-ion batteries with electrochemical overpotentials including diffusion," *J. Power Sources*, vol. 500, no. 229991, 2021.

[16] A. Wang, S. Kadam, H. Li, S. Shi, and Y. Qi, "Review on modeling of the anode solid electrolyte interphase (SEI) for lithium-ion batteries," *NPJ Computational Materials*, vol. 4, no. 15, 2018.

[17] P. Ramadass, B. Haran, P. M. Gomadam, R. White, and B. N. Popov, "Development of first principles capacity fade model for li-ion cells," *J. Electrochem. Soc.*, vol. 151, no. 2, pp. A196–A203, 2004.

[18] K. Kanamura, Y. Yamada, K. Annaka, N. Nakata, and H. Munakata, "Electrochemical evaluation of active materials for lithium ion batteries by one (single) particle measurement," *Electrochemistry*, vol. 84, no. 10, pp. 759–765, 2016.

[19] G. Plett, "ECE4710/5710, equivalent-circuit cell models," *University of Colorado*, 2016.

[20] Tesla. (2022) Powerwall 2 datasheet. [Online]. Available: https://www.tesla.com/sites/default/files/pdfs/powerwall/Powerwall%202_AC_Datasheet_en_northamerica.pdf

[21] Center for Advanced Life Cycle Engineering, University of Maryland. (2015) Cylindrical cells: INR18650-20R. [Online]. Available: https://web.calce.umd.edu/batteries/data.htm

[22] Department of Energy and Climate Change, UK. (2014) Household electricity survey. [Online]. Available: https://www.gov.uk/government/publications/household-electricity-survey--2

[23] Public Service Enterprise Group. (2022) Value of distributed energy. [Online]. Available: https://www.psegliny.com/businessandcontractorservices/businessandcommercialsavings/greenenergy/vder

[24] National Renewable Energy Laboratory. (2022) National solar radiation database. [Online]. Available: https://nsrdb.nrel.gov/

[25] New York Independent System Operator. (2022) Energy market & operational data. [Online]. Available: https://www.nyiso.com/energy-market-operational-data

[26] C. Bordin, H. O. Anuta, A. Crossland, I. L. Gutierrez, C. J. Dent, and D. Vigo, "A linear programming approach for battery degradation analysis and optimization in offgrid power systems with solar energy integration," *Renewable Energy*, vol. 101, pp. 417–430, 2017.

[27] S. Lamp and M. Samano, "Large-scale battery storage, short-term market outcomes, and arbitrage," *Energy Economics*, vol. 107, no. 105786, 2022.